Photoacoustics 28 (2022) 100408

Contents lists available at ScienceDirect

Photoacoustics

journal homepage: www.elsevier.com/locate/pacs

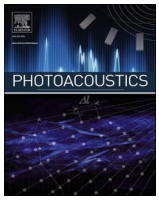

Posterior photoacoustic/ultrasound imaging of the periodontal pocket with a compact intraoral transducer

Lei Fu [a], Reza Khazaeinezhad [b], Ali Hariri [b], Baiyan Qi [c], Casey Chen [d], Jesse V. Jokerst [a,b,c,e,*]

[a] Department of NanoEngineering, University of California San Diego, La Jolla, CA 92093, USA
[b] StyloSonic LLC, Lake Forest, CA 92630, USA
[c] Materials Science and Engineering Program, University of California San Diego, La Jolla, CA 92093, USA
[d] Herman Ostrow School of Dentistry, University of Southern California, 925 West 34th Street, Los Angeles, CA 90089, USA
[e] Department of Radiology, University of California San Diego, La Jolla, CA 92093, USA

ARTICLE INFO

Keywords:
Photoacoustic imaging
Periodontitis
Clinical attachment loss
Oral health
Optoacoustics

ABSTRACT

Periodontitis is a public issue and imaging periodontal pocket is important to evaluate periodontitis. Regular linear transducers have limitations in imaging the posterior teeth due to their geometry restrictions. Here we characterized a transducer that can image the posterior teeth including assessment of periodontal pockets *via* a combination of photoacoustic and ultrasound imaging. Unlike conventional transducer design, this device has a toothbrush-shaped form factor with a side-view transducer to image molars (total size: 1 ×1.9 cm). A laser diode was integrated as the light source to reduce the cost and size and facilitates clinical transition. The *in vivo* imaging of a molar of a periodontal patient demonstrated that the transducer could image in the posterior area of gum *in vivo*; the value determined by imaging was within 7 % of the value measured clinically.

1. Introduction

Periodontitis is a common disease caused by subgingival bacteria that destroy the supporting structures of the teeth [1]. Deeper periodontal probing depths and gingival inflammation are common features of periodontitis [2]. Oral health professionals measure probing depths with a metallic probe placed in the pocket between the gingiva and tooth [3]. However, periodontal probing is subjective to the probing force, probe angulation, and the insertion point [4,5]. Periodontal probing can also cause bleeding and is painful to the patient and time-consuming for the provider.

We previously reported photoacoustic/ultrasound imaging to image the periodontal pocket in an *ex vivo* swine model and *in vivo* human subjects [6,7]. However, only anterior human teeth could be imaged because of the bulky geometry of the transducer. The handle of regular linear transducer needs to project out orthogonally from the tissue surface that is being imaged, which makes the transducer cumbersome to operate in the posterior area of gum. Unfortunately, most periodontitis occurs on posterior teeth including molars and pre-molars. Although there are clinical and small transducers *e.g.*, endoscopic transducers that could be potentially adapted for periodontal imaging [8], they usually have low central frequency at around 5 MHz, which is insufficient to resolve small structures of tooth [9,10]. For this reason, it is important to develop a photoacoustic/ultrasound transducer that can image posterior teeth with high resolution. Concurrently to this, we were motivated to use a light source that is rugged and affordable. While our prior work used a Q-switched laser, such lasers are very expensive and bulky [6,7]. In recently years, many groups have developed laser-diode or LED-based photoacoustic imaging system which is more portable and affordable than Q-switch laser [11].

In this work, we characterized a compact and affordable photoacoustic/ultrasound transducer for *in vivo* full-mouth periodontal pocket imaging. The transducer has a form factor reminiscent of a toothbrush and thus can image all the human teeth *in vivo*. It integrates a 19-MHz ultrasound transducer with optical modules for photoacoustic imaging. We reduced the cost of the system by using laser diode as light source. Here, we first describe the transducer and considerations of using it to image posterior teeth. We then characterized the performance of the whole system in photoacoustic imaging. Finally, we imaged swine teeth *ex vivo* and a molar of a periodontal patient *in vivo*.

* Corresponding author at: Department of NanoEngineering, University of California San Diego, La Jolla, CA 92093, USA.
E-mail addresses: reza@stylosonic.com (R. Khazaeinezhad), jjokerst@ucsd.edu (J.V. Jokerst).

https://doi.org/10.1016/j.pacs.2022.100408
Received 14 April 2022; Received in revised form 15 August 2022; Accepted 25 September 2022
Available online 26 September 2022

2. Materials and methods

2.1. Hardware

We used a high-frequency ultrasound transducer (SS-19–128, StyloSonic, USA) in a custom handpiece. It has central frequency of 19 MHz and average − 6 dB bandwidth of 48.9 %. The transducer has 128 elements with element pitch of 78 μm. The laser diode generates laser pulses in 1 kHz in 808 nm. The pulse energy is 0.7 mJ/cm^2 after coupling and the pulse width is 100 ns. A research ultrasound data acquisition system (Vantage; Verasonics, Inc., Kirkland, WA, USA) was used to receive, process, and reconstruct the photoacoustic/ultrasound signals. The Vantage system has 256 channels with maximum sampling rate of 62.5 MHz. It provides output triggers to synchronize with the laser diode.

2.2. Data acquisition and processing

We performed real-time interleaved photoacoustic and ultrasound imaging [12,13]. The sampling rate was 41.67 MHz in photoacoustic imaging and 62.5 MHz in ultrasound imaging. The ultrasound DAQ triggered the laser diode each time and also acquired data during PA imaging. The photoacoustic RF data were averaged 20 times before reconstruction. We used a beamforming method named 'wide beam' for ultrasound imaging [14]. The ultrasound and PA images were reconstructed by the software in the commercial DAQ system in real time (Vantage, Verasonics). We overlaid the PA image on the ultrasound image during postprocessing. The PA signal in red scale was thresholded and weighted before being overlaid on the ultrasound signal in gray scale.

2.3. Characterization

Characterizations of photoacoustic imaging used a tissue-mimicking phantom made by 20 % intralipid solution. We used pencil leads (0.2 mm diameter) to evaluate light homogeneity. We used a photodetector (PE50-DIF-C, Ophir Photonics Corporation) connected with an oscilloscope (SDS 1202X-E, Siglent Inc.) to measure the light stability. Three polyethylene tubes filled with cuttlefish ink were used to evaluate the imaging depth of the transducer. A human hair (0.1 mm diameter) was used to evaluate the resolution of photoacoustic imaging. A nichrome wire (0.03 mm diameter) was used to evaluate the resolution of ultrasound imaging.

2.4. Swine teeth

Swine jaws were obtained from a local abattoir. One swine tooth (1st molar) was prepared for the ultrasound imaging in Fig. 3, and two more swine teeth (1st molar and 1st pre-molar) were prepared for photoacoustic/ultrasound imaging in Fig. 4.

2.5. Contrast agent

The melanin nanoparticles in the cuttlefish ink (Nortindal, Spain) were used as a photoacoustic contrast agent to highlight the pocket as described by us previously in both swine and humans [6,7]. Cuttlefish ink is a food ingredient that contains melanin nanoparticles, water, salt, and sodium carboxymethyl cellulose. Cuttlefish ink solution was diluted in a solution containing 5 % ink w/v in water. Our previous work showed that the melanin particles are flat absorbers [7]. The periodontal pocket of swine and human teeth were labelled with ~8 μL of contrast agent per tooth. A micropipette containing the contrast agent with a sterile 2–20 μL tip was placed in contact with the gingival margin to irrigate the sulcus with contrast agent. The contrast agent on the teeth was removed with sterile cotton swabs and residual ink was removed by toothbrushing after imaging.

2.6. Periodontal pocket imaging

The photoacoustic images were collected along with ultrasound data for anatomy. The photoacoustic image shows the distribution of the contrast agent in the pocket and was used to measure pocket depth. Pocket depth measurements were measured by Marquis probing method and photoacoustic method. The Marquis probe has black/white rings marking the probing depth. The probe was placed into the pocket along the direction of tooth root [15] for conventional probing assessment.

2.7. Ultrasound coupling

An ultrasound gel pad (Parker laboratories, Inc., USA) was placed between the optical window and mirror. We used a gel pad for ultrasound coupling and more importantly created a space between the optical window and tissue for light coupling. A layer of tegaderm was used to wrap and fix the gel pad. Sterile ultrasound gel (Parker laboratories, Inc.) was used on the exterior of the parafilm wrap to facilitate coupling to the gum and teeth.

2.8. Participant

All work with human subjects was approved by the University of California – San Diego (UCSD) and University of Southern California (USC) IRBs and conducted according to the ethical standards set forth by the IRB and the Helsinki Declaration of 1975. The participant gave written informed consent and teeth were imaged non-invasively. All subjects were > 18 years old and able to provide consent. One healthy subject and one periodontal patient were recruited for this study. The imaging of periodontal patient was handled by a board-certified periodontist (author CC) at USC dental school.

3. Results and discussion

We first describe the device (Fig. 1) and characterized the performance of the transducer in photoacoustic imaging (Fig. 2), and then validated its performance in ultrasound imaging (Fig. 3). We eventually performed both *ex vivo* and *in vivo* periodontal pocket imaging (Fig. 4).

3.1. Device

The periodontal imaging system includes a photoacoustic/ultrasound imaging transducer, a laser-diode module, and a research-based ultrasound DAQ system (see Methods for configurations) (Fig. 1(A)). Photoacoustic imaging requires optical excitation, and the transducer integrates a transparent window and mirror for light delivery for photoacoustic imaging. This device uses a laser-diode module that delivers light to the transducer *via* an optical fiber. The transducer receives the photoacoustic and ultrasound signals which are processed by the DAQ system. A supplementary video is shared online that shows the operation of the system in periodontal pocket imaging (https://youtu.be/PwSrq0kDJuc).

The laser-diode module contains a custom-designed pulsed laser diode, a function generator board, coupling lens, and a heat sink (Fig. 1 (B)). The laser-diode module's dimensions are 35 cm (length) × 19 cm (width) × 28 cm (height), and it weighs ~5 kg. The laser diode generates 1-kHz laser pulses that are coupled into the fiber and delivered remotely to the transducer for photoacoustic imaging. Thus, the transducer side (Fig. 1(C)) does not have any light source or heat sink, thus making the transducer more compact than LED-based systems. Alternative LED-based photoacoustic imaging systems require the LED arrays and heat sink to be assembled on the transducer which increase the size [16]. Custom-designed coupling optics was utilized to collimate the light pulse with a high angle of divergence into the delivery optical fiber with a core diameter of 1.5 mm and a 0.5 numerical aperture (NA). This design directs the light from the coupling design to the end of the

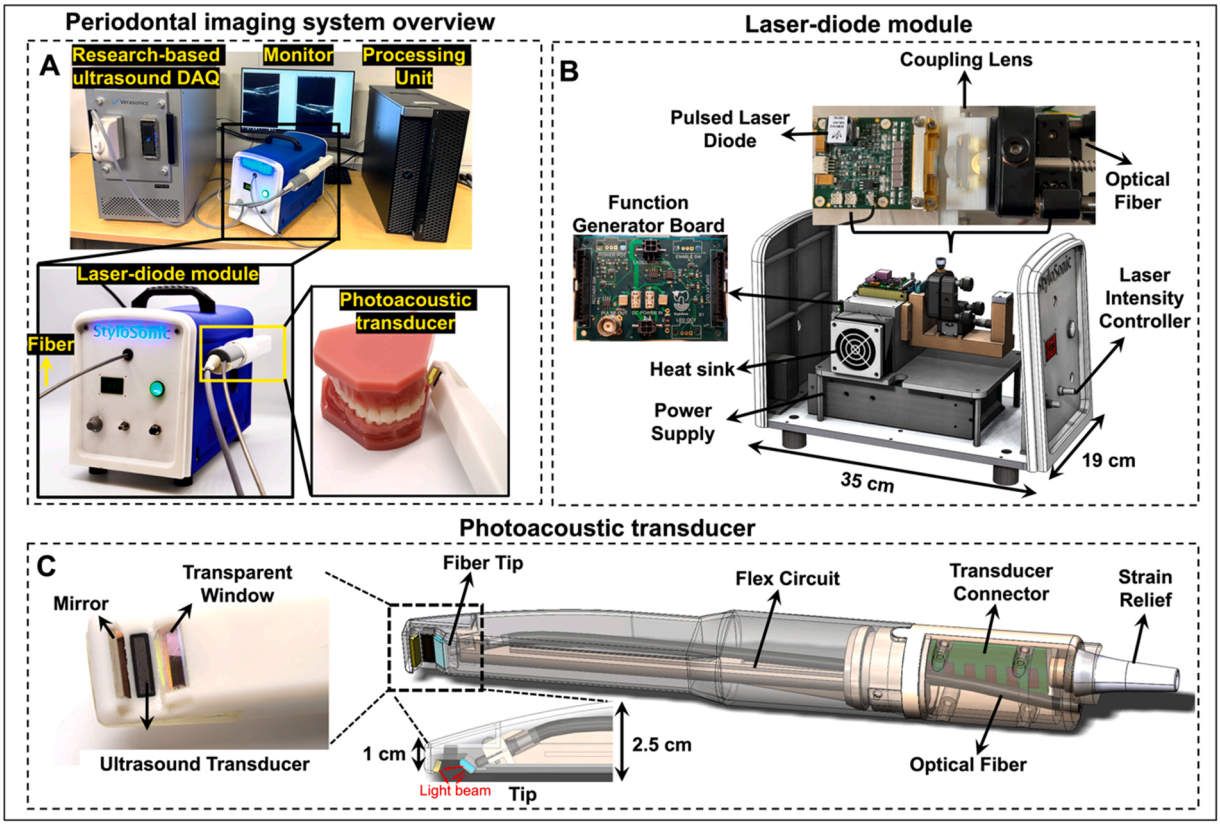

Fig. 1. Full-mouth periodontal imaging system. A) System overview. A laser-diode module is the light source and light pulses are delivered to the transducer *via* a fiber. The transducer is integrated into a handheld device. A research-based ultrasound DAQ system processed and reconstructed the photoacoustic/ultrasound signals. B) A laser-diode module houses the pulsed laser diode, coupling lens, customized function generator board, heat sink, and power supply. The front panel has the control button to adjust the laser intensity. C) The photoacoustic transducer includes an ultrasound transducer, transducer connector, flex circuit, an optical fiber, transparent window, and mirror. The small tip of the handpiece (10 mm × 19 mm) facilities full-mouth scanning.

handpiece. The pulse energy is 4 mJ before the coupling and 0.74 mJ after the coupling. The laser-diode module also provides trigger in & out channels through a function generator board for synchronization. The laser-diode module is also more compact than a regular Q-switch laser, which makes it suitable for chairside imaging [17]. One limitation of the laser diode is that the pulse width is 100 ns, and thus it generates most of the photoacoustic signal below 10 MHz [18]; noise starts to dominate the photoacoustic signal in the high-frequency domain. However, high-frequency transducers can help identify the small features of the oral anatomy in ultrasound imaging. For these reasons, we used the lower half of the 19 MHz transducer bandwidth for photoacoustic imaging to reach the best SNR and resolution, and used its full bandwidth for ultrasound imaging.

The transducer integrates the 19-MHz ultrasound transducer (average −6 dB bandwidth of 48.9 %) facing towards the tissue while the handle can project out from the gum parallel to the tissue surface (Fig. 1(C)). This toothbrush-shaped design can image the posterior teeth in contrast to conventional transducers [19,20]. A transparent window was placed on the tip of the handpiece to protect the components. The fiber inside the transparent window was tilted and can illuminate the light onto the gum. Furthermore, a gold-coated mirror reflects the scattered light back to the tissue surface to maximize the fluence for photoacoustic imaging.

3.2. Characterization

We characterized the light homogeneity, light stability, penetration depth, and resolution of the system for photoacoustic imaging. The periodontal pocket and its associated tissue are less than 10 mm across the gingiva and tooth, and less than 4 mm deep from the gingiva surface. An array of pencil leads (10 mm wide, 5 leads) was put in a phantom solution (see Methods) 8 mm below the transducer to examine the light homogeneity. Pencil leads are strong light absorber, and their photoacoustic intensity correlates well with the local light intensity [21]; stronger photoacoustic signal indicates stronger light focus. All five pencil leads are distinguishable in the 10-mm range in the photoacoustic image with similar intensity (Fig. 2(A)). Fig. 2(A) shows the statistics that the photoacoustic intensity of the 5 pencil leads have only 11 % relative standard deviation (RSD), which indicates uniform illumination.

We also measured the stability of the laser diode by monitoring its intensity in one hour duration (Fig. 2(B)). The light intensity dropped from 0.74 mJ/cm^2 to 0.58 mJ/cm^2 in the one hour with 20 % variation. Three polyethylene tubes loaded with 20 μL contrast agent (cuttlefish ink solution) were fixed by a 3D printed holder. They were put in the phantom at different depths (7 mm, 11 mm, and 15 mm) from the transducer. The first two tubes are distinguishable while the third is barely observable with photoacoustic imaging (Fig. 2(c)). Fig. 2(C) shows that the signal-to-noise ratio (SNR) decreases with imaging depth which is expected due to light attenuation. These results demonstrate that the system can image contrast agents as deep as 11 mm in tissue with more than 10-dB SNR. The pulse energy of the laser diode is sufficient for periodontal pocket imaging (less than 4 mm deep).

The lateral and axial resolution of the system in photoacoustic imaging were determined by imaging the cross-section of a human hair (100-μm diameter). We defined the FWHM (full width at half maximum) of the lateral and axial amplitude distributions as the axial and lateral resolution, respectively [22]. The lateral and axial amplitude

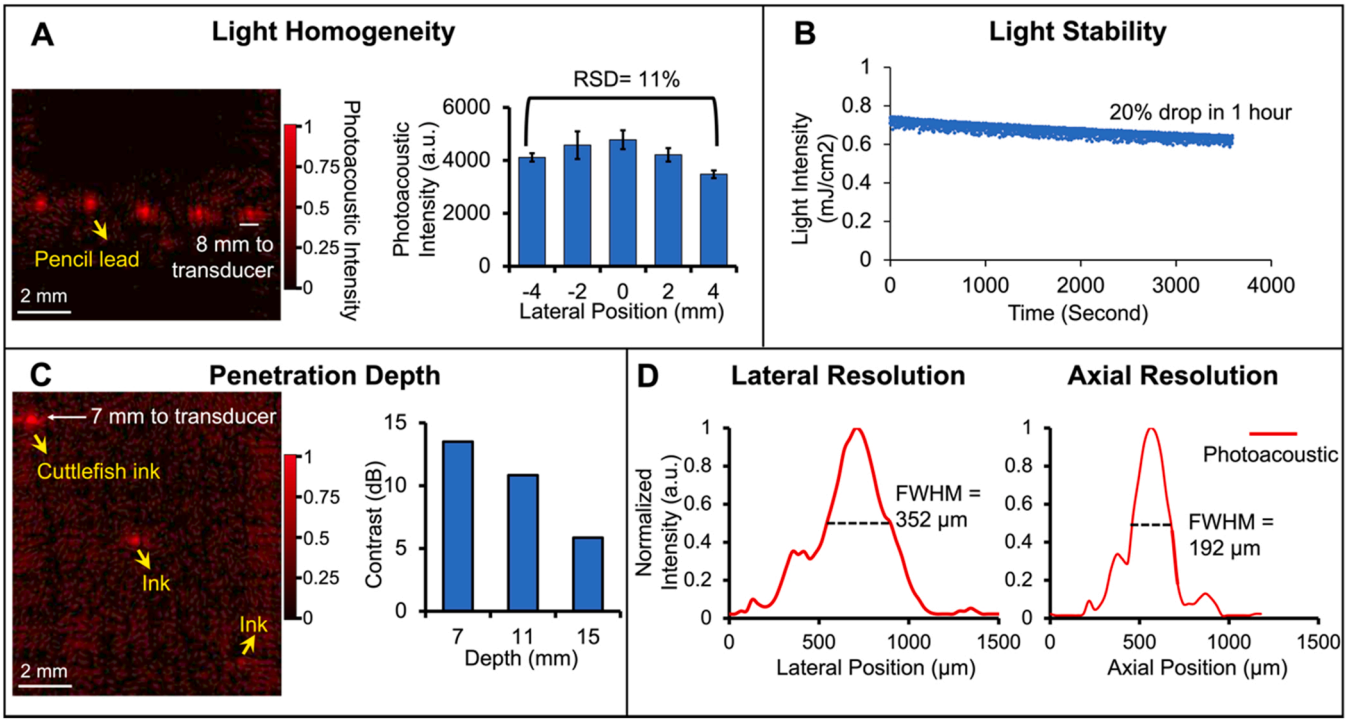

Fig. 2. Performance characterization of the periodontal imaging transducer. A) Light homogeneity evaluation. Photoacoustic imaging of five pencil leads placed parallel over 10 mm and 8 mm under the transducer. The chart shows the relative standard deviation (RSD) of the photoacoustic intensity of the five pencil leads. B) Laser-diode power stability *versus* time in 1-hour scale. C) Imaging depth evaluation. Three tubes containing the contrast agent are put in a tissue mimic phantom located at different depths of 7 mm, 11 mm, and 15 mm from the transducer. The right chart shows the SNRs of the three tubes. D) The lateral and axial photoacoustic amplitude distributions along a 100-μm hair: 352 μm and 192 μm are the lateral and axial resolution in photoacoustic mode, respectively.

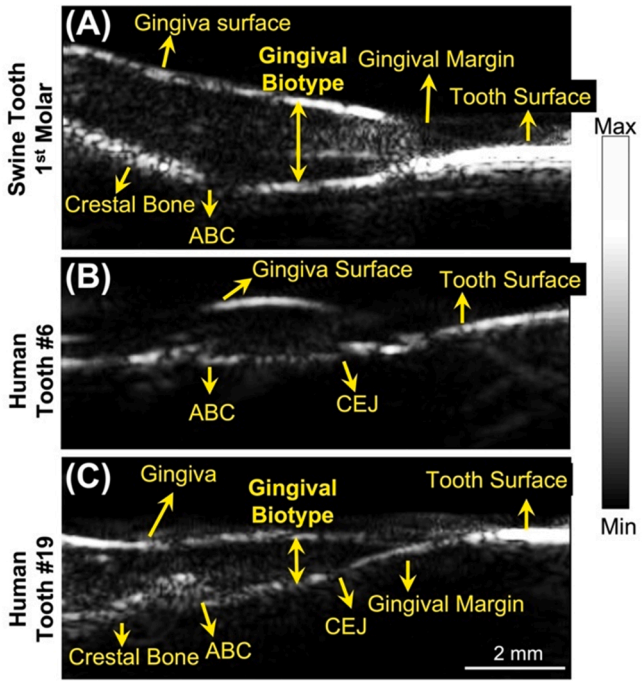

Fig. 3. Ultrasound imaging of swine and human teeth. A-C) are ultrasound images of a swine 1st pre-molar (A), a human cuspid #6 (B), and a human 1st molar #19 (C). All the images are in sagittal view. Alveolar bone crest (ABC). Cementoenamel junction (CEJ).

distributions across the hair were extracted (Fig. 2(D)), and the lateral and axial resolution in photoacoustic mode were 192 μm and 352 μm, respectively. The lateral and axial resolution values in ultrasound-only mode were 142 μm and 102 μm by imaging a 30-μm nichrome wire.

3.3. Ultrasound imaging of swine and human teeth

We next evaluated the performance of the transducer in tooth in ultrasound mode. One swine tooth and two human teeth were imaged *ex vivo* and *in vivo*, respectively. Swine teeth are a common model because they have a similar structure as human teeth [23]. The transducer resolves the structures in both the swine tooth imaging (1st molar, Fig. 3 (a)) and the human tooth imaging (Cuspid #6, Fig. 3(b)) including gingival surface, tooth surface (occlusal surface), gingival margin, alveolar bone, and alveolar bone crest (ABC). The tooth surface has stronger ultrasound intensity because it has higher impedance than other tissue. Moreover, the cementoenamel junction (CEJ) is distinguishable in the human tooth (Fig. 3(b)). Resolving these structures and their positions are very helpful to the diagnosis of periodontal diseases [15]. Moreover, we imaged the 1st molar of a human subject (Fig. 3(c)) *in vivo*. Those structures labeled in Fig. 3(a) and (b) are also observable in Fig. 3(c), which demonstrated that the toothbrush-shaped transducer can operate in the posterior area to image molars *in vivo*, which could be a big challenge for other ultrasound transducers.

3.4. Photoacoustic/Ultrasound imaging of swine and human teeth

We performed photoacoustic/ultrasound dual-mode imaging to resolve the periodontal pockets both *ex vivo* and *in vivo*. We used cuttlefish ink solution as photoacoustic contrast agent which highlights the pocket area. The ultrasound image in grayscale shows the tooth structure, and the photoacoustic image in red scale reveals the contrast agent *i.e.*, the periodontal pocket. Photoacoustic/ultrasound images are

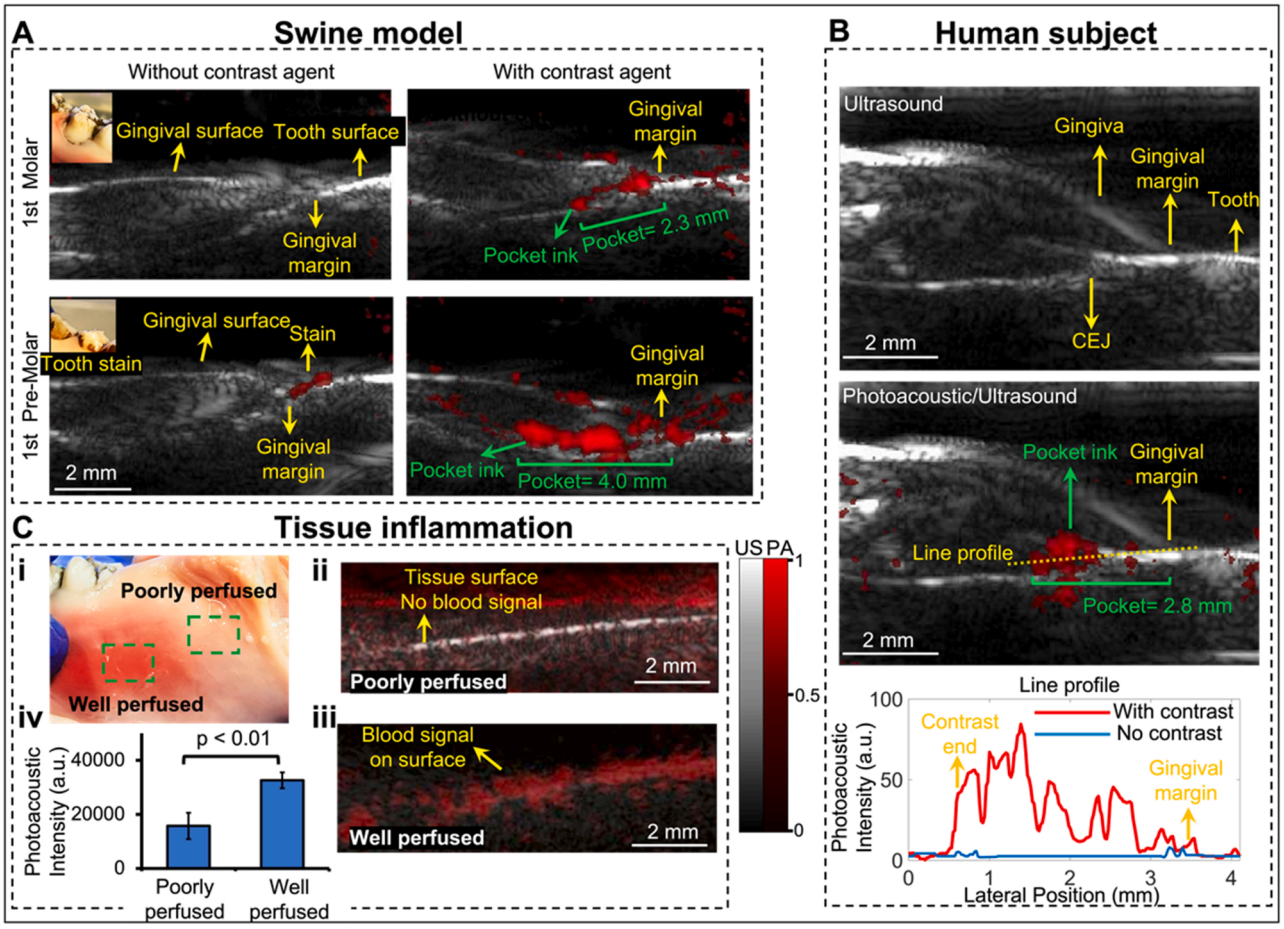

Fig. 4. Periodontal pocket and gingiva inflammation imaging. A) Pocket depth measurement of two swine teeth before and after using the contrast agent. The insets show stains on tooth. Photoacoustic image in red scale is overlaid to ultrasound image in gray scale. All the panels share the same colormap scale. B) Pocket depth measurement of 1st molar #14 of a periodontal patient. The top panel is an ultrasound image of the molar. The middle panel is the photoacoustic/ultrasound image after applying the contrast agent. The bottom panel shows the line profile of the photoacoustic intensity in the pocket. C) Inflammation imaging. Panel i shows the swine gingiva with well-perfused tissue and poorly perfused tissue. Panel ii shows a photoacoustic/ultrasound image of the poorly perfused tissue. Panel iii shows photoacoustic/ultrasound image of the well-perfused tissue. Panel iv is the statistics that shows the overall photoacoustic intensity of healthy tissue (poorly perfused) and inflamed tissue (well perfused).

overlaid together. Two swine teeth (1st pre-molar and 1st molar) were imaged *ex vivo* (Fig. 4(A)) and a molar of a periodontal patient was imaged *in vivo* (Fig. 4(B)). Fig. 4(A) shows the photoacoustic/ultrasound images of the two swine teeth before applying the contrast agent (left panels) and after (right panels). Clearly, there is no photoacoustic signal in the periodontal pocket before applying the contrast agent (left panels). The photoacoustic signal from the 1st pre-molar image was caused by the tooth stain as shown in the inset photo. After applying the contrast agent, the contrast agent is seen as a line below the gingival margin, *i.e.*, the periodontal pocket. This confirms that the photoacoustic transducer can detect the periodontal pocket *ex vivo*. By drawing a line between the gingival margin in the ultrasound image and the contrast end in the pocket in the photoacoustic image, we measured the pocket depth to be 2.3 mm for the 1st molar and 4.0 mm for the 1st pre-molar, which is close to 2 mm and 4 mm respectively by using a clinical periodontal probe.

We further imaged the 1st molar #14 of a periodontal patient (Fig. 4(B)). The diseased patient was diagnosed with stage 2, grade B periodontitis. Tooth #14 was characterized *via* conventional probing. The probing pocket depth (PPD) depths were (from distal to medial to mesial) 4–3–5 mm on the buccal side and 4–3–6 mm on the lingual. The Clinical attachment level (CAL) buccal (from distal to medial to mesial) was 4–3–5 mm, and the CAL lingual was 4–3–6 mm. Similar to the swine teeth, the photoacoustic signal shows up in the pocket after applying the contrast agent (Fig. 4(B)). Fig. 4(B) also shows the line distributions of the photoacoustic signal across the pocket. As can be seen, the pocket area has much stronger photoacoustic intensity (red line) after applying the contrast agent. The pocket depth is measured as 2.8 mm (medial, buccal side). Importantly, our imaging assessment of the probing depth occurred medially is within 7 % of the value (3 mm) determined by using a periodontal probe invasively. The results demonstrate that the transducer can image the periodontal pocket of molars *in vivo*.

Besides periodontal pocket, gingival inflammation also occurs with periodontal disease [24]. It is expected the inflamed tissue is well perfused and hence has more blood signal than healthy tissue (poorly perfused), which can be detected by imaging the hemoglobin by photoacoustic imaging. We performed photoacoustic imaging of the well perfused tissue and poorly perfused (healthy) tissue of the swine tooth model, separately (Fig. 4(C). i). As can be seen, well perfused tissue has much stronger PA signal close to the gingiva surface (Fig. 4(C). ii)) than poorly tissue (Fig. 4(C). iii)). The statistics in Fig. 4(C). iv shows that the overall photoacoustic intensity of the well perfused tissue is around two times higher than the poorly perfused tissue.

There are several limitations in this study. The laser diode is rugged and reduces the costs and size of the imaging equipment—these features facilitate clinical translation relative to the Q-switched laser; however, the laser diode has less pulse energy and longer pulse widths—this limits the bandwidth of the transducers that can be used. In general, longer

pulse widths (100 ns) generate less high-frequency photoacoustic signal (>10 MHz) [18]. Noise starts to dominate the photoacoustic signal in the high-frequency domain. For this reason, laser diodes are suitable primarily for transducers with lower frequency. Nonetheless, it is important to use a high-frequency transducer (30–50 MHz) in periodontal imaging as it can help identify the small features of the oral anatomy in ultrasound imaging [6]. In this work, we made a trade-off between the ultrasound imaging and laser-diode based photoacoustic imaging by using a 19-MHz transducer. We used the lower half of the transducer bandwidth for photoacoustic imaging to collect as much photoacoustic signal as possible in photoacoustic imaging and used the full transducer bandwidth in ultrasound imaging for higher resolution.

Other limitations include gel coupling, which is cumbersome in clinical practice. In the *in vivo* human study (Fig. 4(B)), the ultrasound coupling process took 3–5 min, which includes applying ultrasound gel, optimizing ultrasound coupling, and cleaning the gel from the oral space. The ultrasound/photoacoustic images were acquired within seconds. The community has recently reported solid-phase couplants to facilitate acoustic imaging in the mouth [25], and these will be used in future work. A third limitation of this technique is the use of the exogenous contrast agent. Cuttlefish ink can have an odor and is contraindicated in subjects with a seafood allergy; alternative agents include the activated charcoal used as a tooth-whitening product. Finally, although we have proven that the photoacoustic imaging method has good correlation to gold standard methods in a swine model, factors that might affect the accuracy of this method include the tilt angle of the transducer, and the penetration depth of the contrast agent in deep pockets (> 5 mm) [26]. Thus, more clinical replicates are still needed. We have shown that single irrigation of the sulcus can map the entire periodontal pocket of a single tooth [6], single irrigation for all teeth mapping *in vivo* has yet to be shown. Ongoing work is integrating this irrigation process with standard cleaning protocols.

4. Conclusion

In conclusion, we evaluated a tooth-brushed-shaped photoacoustic/ultrasound transducer for full-mouth periodontal pocket imaging. The unique tooth-brush design allows the transducer to fit in the posterior area of gum and image molars. The device uses a laser diode as the light source to reduces the costs. We performed *ex vivo* swine teeth imaging and *in vivo* periodontal patient imaging. The results demonstrated the transducer can image the periodontal pocket in molars *in vivo*.

Funding

A.H. and R.K. acknowledge R43 DE031196. J.V.J acknowledges R21 DE029025 and UL1 TR001442.

Disclosures

R.K., A.H., and J.V.J. are co-founders of StyloSonic, LLC.

Declaration of Competing Interest

The authors declare that they have no known competing financial interests or personal relationships that could have appeared to influence the work reported in this paper.

Data Availability

Data will be made available on request. Data can be requested from the authors at any time. A supplementary video is shared online that shows the operation of the system in periodontal pocket imaging (https://youtu.be/PwSrq0kDJuc).

References

[1] NHNES, OH-5 Reduce the proportion of adults aged 45 to 74 years with moderate or severe periodontitis, ⟨https://www.healthypeople.gov/2020/data/Chart/5026?category=1&by=Total&fips=-1⟩.
[2] F.F. Farook, H. Alodwene, R. Alharbi, M. Alyami, A. Alshahrani, D. Almohammadi, B. Alnasyan, W. Aboelmaaty, Reliability assessment between clinical attachment loss and alveolar bone level in dental radiographs, Clin. Exp. Dent. Res 6 (2020) 596–601.
[3] S. Khan, L.L. Cabanilla, Periodontal probing depth measurement: a review, Compend Contin. Educ. Dent. 30 (2009) 12–14, 16, 18-21; quiz 22, 36.
[4] C. Larsen, D.S. Barendregt, D.E. Slot, U. Van der Velden, F. Van der Weijden, Probing pressure, a highly undervalued unit of measure in periodontal probing: a systematic review on its effect on probing pocket depth, J. Clin. Periodo 36 (2009) 315–322.
[5] A.J. Biddle, R.M. Palmer, R.F. Wilson, T.L. Watts, Comparison of the validity of periodontal probing measurements in smokers and non-smokers, J. Clin. Periodo 28 (2001) 806–812.
[6] C. Moore, Y. Bai, A. Hariri, J.B. Sanchez, C.Y. Lin, S. Koka, P. Sedghizadeh, C. Chen, J.V. Jokerst, Photoacoustic imaging for monitoring periodontal health: a first human study, Photoacoustics 12 (2018) 67–74.
[7] C.Y. Lin, F. Chen, A. Hariri, C.J. Chen, P. Wilder-Smith, T. Takesh, J.V. Jokerst, Photoacoustic imaging for noninvasive periodontal probing depth measurements, J. Dent. Res 97 (2018) 23–30.
[8] M. Giovannini, S. Ardizzone, Anorectal ultrasound for neoplastic and inflammatory lesions, Best. Pr. Res Cl. Ga 20 (2006) 113–135.
[9] K.C.T. Nguyen, L.H. Le, N.R. Kaipatur, R. Zheng, E.H. Lou, P.W. Major, High-resolution ultrasonic imaging of dento-periodontal tissues using a multi-element phased array system, Ann. Biomed. Eng. 44 (2016) 2874–2886.
[10] K.C.T. Nguyen, B.M. Le, M.X. Li, F.T. Almeida, P.W. Major, N.R. Kaipatur, E.H. M. Lou, K. Punithakumar, L.H. Le, Localization of cementoenamel junction in intraoral ultrasonographs with machine learning, J. Dent. 112 (2021).
[11] A. Fatima, K. Kratkiewicz, R. Manwar, M. Zafar, R.Y. Zhang, B. Huang, N. Dadashzadeh, J. Xia, K. Avanaki, Review of cost reduction methods in photoacoustic computed tomography, Photoacoustics 15 (2019).
[12] L. Fu, Z.C. Jin, B.Y. Qi, W.J. Yim, Z.H. Wu, T.Y. He, J.V. Jokerst, Synchronization of RF data in ultrasound open platforms (UOPs) for high-accuracy and high-resolution photoacoustic tomography using the "scissors" programming method, IEEE T Ultrason Ferr. 69 (2022) 1994–2000.
[13] W.C. Zhang, J.D. Li, S.H. Yang, Real-time interleaved photoacoustic and ultrasound imaging for guiding interventional procedures, Appl. Acoust. 156 (2019) 1–6.
[14] G. Matrone, A.S. Savoia, G. Caliano, G. Magenes, Ultrasound plane-wave imaging with delay multiply and sum beamforming and coherent compounding, Ieee Eng. Med Bio (2016) 3223–3226.
[15] O.D.K. Hsun-Liang (Albert) Chan, Dental Ultrasound in Periodontology and Implantology, Springer, 2020.
[16] A. Hariri, J. Lemaster, J.X. Wang, A.S. Jeevarathinam, D.L. Chao, J.V. Jokerst, The characterization of an economic and portable LED-based photoacoustic imaging system to facilitate molecular imaging, Photoacoustics 9 (2018) 10–20.
[17] M. Erfanzadeh, Q. Zhu, Photoacoustic imaging with low-cost sources; a review, Photoacoustics 14 (2019) 1–11.
[18] T. Agano, N. Sato, and K. Awazu, LED-based photoacoustic imaging system - why it achieves the same signal to noise ratio as solid-state-laser-based system; A review, Photons Plus Ultrasound: Imaging and Sensing 2020 **11240** (2020).
[19] K. Sinjab, O.D. Kripfgans, A. Ou, H.L. Chan, Ultrasonographic evaluation of edentulous crestal bone topography: a proof-of-principle retrospective study, Oral. Surg. Oral. Med Oral. Pathol. Oral. Radio. 133 (2022) 110–117.
[20] M. Tattan, K. Sinjab, E. Lee, M. Arnett, T.J. Oh, H.L. Wang, H.L. Chan, O. D. Kripfgans, Ultrasonography for chairside evaluation of periodontal structures: a pilot study, J. Periodo 91 (2020) 890–899.
[21] A. Hariri, K. Alipour, Y. Mantri, J.P. Schulze, J.V. Jokerst, Deep learning improves contrast in low-fluence photoacoustic imaging, Biomed. Opt. Express 11 (2020) 3360–3373.
[22] X. Li, W. Wei, Q. Zhou, K.K. Shung, Z. Chen, Intravascular photoacoustic imaging at 35 and 80 MHz, J. Biomed. Opt. 17 (2012), 106005.
[23] F.I. Tsiolis, I.G. Needleman, G.S. Griffiths, Periodontal ultrasonography, J. Clin. Periodo 30 (2003) 849–854.
[24] R.C. Page, H.E. Schroeder, Pathogenesis of inflammatory periodontal disease. A summary of current work, Lab Invest 34 (1976) 235–249.
[25] D. Sun, J. Liu, L.J. Xue, L. Li, D.Y. Xie, S.L. Li, S.M. Li, X.L. Wang, D.T. Yin, Z. Q. Ren, R. Bai, W. Guo, Y. Liu, C.Y. Chen, A solid ultrasonic coupling membrane for superficial vascular ultrasonography, Nanoscale 14 (2022) 3545–3553.
[26] L. Fu, C. Ling, Z.C. Jin, J. Luo, J. Palma-Chavez, Z.H. Wu, J.C. Zhou, J.J. Zhou, B. Donovan, B.Y. Qi, A. Mishra, T.Y. He, J.V. Jokerst, Photoacoustic imaging of posterior periodontal pocket using a commercial hockey-stick transducer, J. Biomed. Opt. 27 (2022).

Jesse V. Jokerst is a Professor in the Department of NanoEngineering at UC San Diego. Dr. Jokerst graduated *cum laude from Truman State University in 2003 with a B.S. in Chemistry and completed a Ph.D. in Chemistry at The University of Texas at Austin in 2009. Jesse was a postdoc at Stanford Radiology from 2009 to 2013 and was an Instructor in that same department from 2013 – 2015. Jesse started at UCSD in July of 2015, and he has received the NIH K99/R00 Pathway to Independence Award, the NIH New Innovator Award, the NSF CAREER Award, and Stanford Radiology Alumni of the Year Award. He is the PI of multiple NIH grants and NSF grants, and serves on the Editorial Advisory Board of ACS Applied Nano Materials and Nanoscale..*

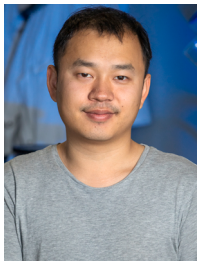

Lei Fu is a PhD student in the Nanoengineering department at UC San Diego. He received his B.S and M.E. degree from Jiangnan University in China. His previous work mainly concentrates on Optical Coherence Tomography(OCT) especially OCT angiography. Currently he is working on photoacoustic periodontal imaging.

Reza Khazaeinezhad, Ph.D., MBA, PMP; Dr. Khazaeinezhad received his PhD in Biomedical Optics and his research focuses on biomedical imaging systems and the development of novel optical technologies/ instrumentation for biomedical research and clinical applications. He has published over 20 peer-reviewed articles, presented in more than 10 major international conferences. He also holds a Medical Device Development Certificate from Harvard's clinical and translational science center, as well as an MBA degree in entrepreneurship from the University of California, Irvine.

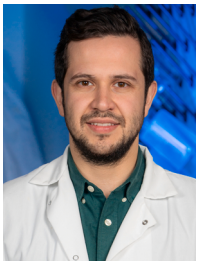

Dr. Hariri received my PhD from the Department of Nanoengineering at UCSD. His research focused on developing, improving, and utilizing low fluence-based photoacoustic imaging systems. His LED-photoacoustic imaging characterization publication in 2018 is one of the most cited articles in Photoacoustic Journal, to date.

Baiyan Qi a PhD student in Materials Science and Engineering program at UCSD. She received her B.S. degree in Physics from Nanjing University in China. Her previous research focused on stretchable wearable electronics. She is currently working on ultrasonic and photoacoustic healthcare imaging.

Dr. Casey Chen is a Professor and Chair, Division of Periodontology, Diagnostic Sciences and Dental Hygiene, Ostrow School of Dentistry of USC. He graduated from National Taiwan University with a degree of BDS in 1980, and has since obtained a certificate in Advanced Periodontology at University of Pittsburgh, a Ph.D. in Oral Biology from State University of New York at Buffalo, and a dental degree from Loma Linda University. Casey is active in clinical and didactic teachings in periodontology as well as in basic science research in microbial pathogenesis. His research interests include genomics and metagenomics of periodontal bacteria, microbial markers of periodontal diseases, virulence determinants of periodontal pathogenic species and clinical therapy of periodontitis.